Contents lists available at ScienceDirect

Soil & Environmental Health

journal homepage: www.sciencedirect.com/journal/soil-and-environmental-health

Research Paper

Effects of pyrolysis temperature on the photooxidation of water-soluble fraction of wheat straw biochar based on 21 T FT-ICR mass spectrometry

Amy M. McKenna [a,b,**], Martha L. Chacón-Patiño [a], Holly K. Roth [b,c], William Bahureksa [d], Robert B. Young [d], James A. Ippolito [e], Yan Xin [f], Thomas Borch [b,c], Antony J. Williams [g], Huan Chen [a,*]

[a] National High Magnetic Field Laboratory, Ion Cyclotron Resonance Facility, Florida State University, 1800 East Paul Dirac Dr., Tallahassee, FL 32310-4005, United States
[b] Department of Soil and Crop Sciences, Colorado State University, Fort Collins, CO 80523-1170, United States
[c] Department of Chemistry, Colorado State University, Fort Collins, CO 80523, United States
[d] Chemical Analysis & Instrumentation Laboratory, New Mexico State University, Las Cruces, NM 88003, United States
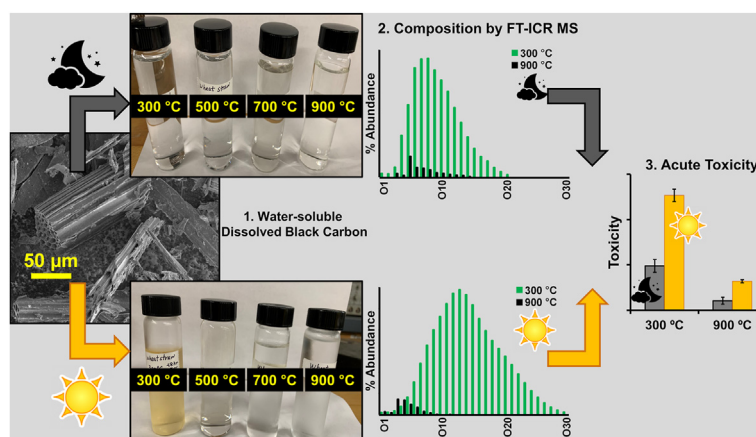[e] School of Environment and Natural Resources, The Ohio State University, Columbus, OH 43210, United States
[f] National High Magnetic Field Laboratory, Magnet Science & Technology, Florida State University, 1800 East Paul Dirac Dr., Tallahassee, FL 32310-4005, United States
[g] Center for Computational Toxicology & Exposure, U.S. Environmental Protection Agency, Research Triangle Park, Durham, NC 27711, United States

HIGHLIGHTS

- Acute toxicity changes as a function of pyrolysis temperature after photoirradiation
- Pyrolysis temperature affects amount and composition of water-soluble biochar species.
- FT-ICR MS identifies molecular signatures of biochar species across pyrolysis temperatures.

GRAPHICAL ABSTRACT

ARTICLE INFO

ABSTRACT

Biochar, formed through the pyrolysis or burning of organic wastes, has a complex chemical composition influenced by feedstock, pyrolysis temperature, and reaction conditions. Water-soluble, dissolved black carbon species released from biochar comprise one of the most photoreactive organic matter fractions. Photodegradation of these water-soluble species from wheat straw biochar, produced at different pyrolysis temperatures in laboratory microcosms, resulted in noticeable compositional differences. This study characterized water-soluble transformation

* Corresponding author.
** Corresponding author. National High Magnetic Field Laboratory, Ion Cyclotron Resonance Facility, Florida State University, 1800 East Paul Dirac Dr., Tallahassee, FL 32310-4005, United States.
E-mail addresses: mckenna@magnet.fsu.edu (A.M. McKenna), huan.chen@magnet.fsu.edu (H. Chen).

Molecular composition
Toxicity assessment
Highly oxidized OC
Surface morphology
Soil organic matter
Pyrolyzed carbon
Aromaticity index
Photoproducts
Black carbon

products formed through the photodegradation of wheat straw biochar pyrolyzed at 300, 400, 500, or 600°C by electrospray ionization 21 T Fourier transform ion cyclotron resonance mass spectrometry (21T FT-ICR MS). We also evaluated global trends in the toxicity of these water-soluble fractions using MicroTox™ to assess the impacts of pyrolysis temperature. Additionally, we examined biochar surface morphology after photodegradation and observed minimal change after irradiation for 48 h, though the total yield of water-soluble biochar species varied with pyrolysis temperature. Trends in toxicity observed from MicroTox® analysis reveal that water-soluble photoproducts from biochar produced at 300°C and 900°C are nearly three times as toxic compared to dark controls. The ultrahigh resolving power of 21T FT-ICR MS allows for the separation of tens of thousands of highly oxidized, low-molecular-weight (<1 kDa) species, showing that photoproducts span a wider range of H/C and O/C ratios compared to their dark analogs. This study highlights the impacts of photodegradation on the molecular composition of water-soluble biochar species and underscores the influence of pyrolysis temperature on the quantity and composition of dissolved organic species.

1. Introduction

Biochar is one type of black carbon – the continuum of solid residues that result from the physical, chemical, and thermal conversion of carbonaceous materials – that includes soot, charcoal, char, and pyrogenic organic matter (Awan et al., 2021). Importantly, biochar in agricultural lands impacts plant growth, soil physicochemical properties, and contaminant stability, with widespread applications that utilize biochar for nutrient replenishment and contaminant remediation in depleted or contaminated soils. In addition, biochar shows promise for carbon sequestration to mitigate climate change while simultaneously improving agricultural yields through the addition of organic and inorganic compounds that enrich soil fertility (Mao et al., 2012; Spokas et al., 2012; Ahmed et al., 2021). Biochar composition and physicochemical properties depend on pyrolysis conditions and feedstock, with the most impact observed on biochar properties at different pyrolysis temperatures (Bednik et al., 2022).

Black carbon is a highly recalcitrant mixture of compounds across a continuum of physical and chemical properties and ranges from slightly charred biomass to soot and charcoal (Coppola et al., 2018). From bulk elemental analysis, atomic H/C and O/C ratios decrease at increased pyrolysis temperatures, resulting in an increased fraction of condensed aromatic species formed through dehydration and condensation reactions (Ward et al., 2014). Conversely, the aliphatic fraction decreases with formation temperature; thus, black carbon is uniquely characterized by hydrogen-deficient condensed ring aromatic species formed at high temperatures (Hockaday et al., 2009). Dissolved black carbon represents the water-soluble fraction of black carbon formed from heating and incomplete combustion of organic matter. This fraction of black carbon can be one of the more photoactive components in the dissolved organic matter (DOM) pool (Ward et al., 2014). Thus, biochar is a form of black carbon that contains a fraction of water-soluble species. Mobilization of these species from biochar into soils or water is influenced by the chemical composition of the feedstock and the pyrolysis temperature and conditions (Ippolito et al., 2020). Some water-soluble species from biochar may pose environmental risks, and thus, biochar applications need to be carefully understood (Godlewska et al., 2021; Xiang et al., 2021; Han H. et al., 2022).

Due to the wide variation in feedstock, pyrolysis conditions, and the polyfunctionality and compositional complexity of various biochar sources, biochar applications for soil remediation can be highly variable (Schmidt et al., 2021). Often applied to low-fertility soils, biochar improves the fertility of unproductive soils, increases crop yields, reduces plant drought stress, sequesters pollutants, and restores agricultural environments, likely due to the presence of black carbon in biochar (Ippolito et al., 2020).

Although biochar has many benefits for soil remediation, pyrolysis of biomass can result in the formation of unwanted toxicants such as polycyclic aromatic hydrocarbons (PAHs)that can result in unwanted contaminant introduction (Wang et al., 2017; Schmidt et al., 2021). Careful modification of feedstock type and pyrolysis temperature enables the tuning of biochar composition to minimize the formation of bioavailable PAHs and other toxic compounds (Liu and Fan, 2022). Solvent extraction methods for PAH identification have been reported to characterize PAH evolution in biochar to serve as a quality control measure prior to biochar application to minimize PAH accumulation and environmental risks (Rombolà et al., 2016). Therefore, biochar selection should be tailored for each application to ensure optimal feedstock, pyrolysis temperature, and residence time to minimize the introduction of deleterious and/or toxic species (Wang et al., 2017). However, most studies that catalogue PAH formation in biochar utilize gas-chromatography, which is limited in detecting species of low volatility (<400 °C) (Dutta et al., 2017). Importantly, compounds introduced to the soil through biochar application degrade through oxidative weathering to transformed products, increasing biochar polarity and water solubility. The composition of biochar feedstock determines the degree of oxidative weathering, thereby dictating the amount and type of water-soluble biochar species that can run off an agricultural field during irrigation or storm events and enter surrounding surface waters, posing a potential threat to downstream users.

Photochemical degradation of natural organic matter occurs through the absorption of photons by organic species, generation of direct photoproducts or triplet excited states, and subsequent reaction with dissolved oxygen that yields reactive oxygen species (e.g., singlet oxygen) or degrades other organic species through electron transfer (Zhang et al., 2021). Ward et al. (2014) studied phototransformation and mineralization of biochar and reported the formation of partially oxidized products through photoreactions. Under solar irradiation, water-soluble biochar species are lower in molecular weight compared to dark analogs, attributed to the photodecomposition of high molecular weight fractions (Chen et al., 2014). Photochemical degradation of biochar-derived dissolved organic matter and organic pollutants have been reported (Zhang et al., 2021). Solar irradiation absorbed by PAH chromophores produces oxidative reactive intermediates that can damage cellular macromolecules, and oxygenated photoproducts are more toxic than precursors (Chen et al., 2022). Reported toxic "oxy-PAHs" include 1,6-benzo[a]pyrenequinone (DTXSID80952917), 3,6-benzo[a]pyrenequinone (DTXSID40952918), and benz[a]anthraquinone (DTXSID8051916) where the DTXSID is the unique substance identifier in the CompTox Chemicals Dashboard (*vide infra*) (Lampi et al., 2009). Bostick et al. highlighted the impact of photoirradiation on leachates from a thermal suite of biochar solids and examined the effect of source/composition and photoirradiation on composition (Bostick et al., 2021). The influence of biochar feedstock and pyrolysis conditions on photogenerated water-soluble species composition has been investigated by several bulk analytical techniques (e.g., nuclear magnetic resonance (NMR), X-ray absorption near edge spectroscopy (XANES)) combined with mass spectrometry (Bostick et al., 2018, 2021; Bahureska et al., 2021).

Over the past two decades, ultrahigh-resolution Fourier transform ion cyclotron resonance mass spectrometry (FT-ICR MS) has become widely applied to molecular characterization of NOM systems (including petroleum, biochar, dissolved/soil/organic matter, terrestrial/marine/lacustrine organic matter) due to its resolving powers in excess of 2,000,000 at m/z 400 that enables resolution of species differ in mass by the mass of an electron. It enables the identification of the mobile fraction

of biochar, and subsequently, the identification of thousands of biochar species. (Bostick et al., 2018, 2021; Wozniak et al., 2020).

The application of FT-ICR MS to natural organic matter systems has helped study the global carbon cycle at the molecular level by identifying tens of thousands of molecular tracers for carbon cycling evaluation (McKenna et al., 2021; Bahureksa et al., 2022; Bare et al., 2023). Here, we investigated the quantitative change in water-soluble carbon derived from wheat straw biochar as a function of pyrolysis temperature (300, 500, 700, and 900 °C) under controlled exposure to simulated sunlight and in the dark. Next, we evaluated the general trends in the global toxicity of the water-soluble fractions of biochar formed from the same feed but produced at varying pyrolysis temperatures. Then, we compared the surface morphology with and without solar irradiation at each temperature after water washing. Finally, we compared the molecular speciation of water-soluble biochar photoproducts with those formed in the dark by negative-ion electrospray ionization 21-T FT-ICR mass spectrometry to catalogue the compositional changes induced by solar irradiation to water-soluble species. Water-soluble biochar species formed at 300 °C correlated to the most toxic fraction, and subsequent comparison of the top 100 most abundant elemental compositions derived from 21 T FT-ICR MS to known toxicants correspond to the same elemental compositions identified as toxicants by the U.S. Environmental Protection Agency. Collectively, we highlight the global trend in the formation of water-soluble biochar species of varying toxicity that occurs concurrent with pyrolysis temperature and the impact of photochemical degradation on the molecular signature of biochar. Notably, the largest change in global toxicity occurred with biochar pyrolyzed at 300 °C. Therefore, careful selection of pyrolysis conditions and feedstock by biochar operators can minimize the deleterious introduction of potential toxicants, specifically at lower pyrolysis temperatures.

2. Materials and methods

2.1. Biochar preparation

Wheat straw feedstock from a field location in Oregon, USA, was ground, dried, and then heated in a pyrolysis chamber (e.g., muffle furnace) in the absence of oxygen at 300, 500, 700, and 900 °C for 1 h based on EPA SOP EEB/MB/2012-01-r0 (Bollman, 2012). Briefly, wheat straw was dried at 60 °C in a drying oven (Blue M Model POM-326E, Thermal Product Solutions, New Columbia, PA) after harvest. Dried biomass was ground in a laboratory mill (Wiley Model ED-5, Thomas Scientific, Swedesboro, NJ, fitted with a 2-mm mesh sieve plate) and stored in plastic bags in a cool, dry location. Biomass was mixed by rotating and shaking the sample bag for approximately 3 min before pyrolysis (Bollman, 2012). Prepared wheat straw biomass the sole feedstock used in this study, was placed into Inconel crucibles and heated in a furnace with inert (nitrogen) atmosphere for specific periods of time at each temperature. All temperatures greater than 300 °C included a two-stage heating protocol, where the first stage heats the furnace to 300 °C and dwells at this temperature for 30 min to slow the rate of pyrolysis and production of volatile organics, followed by the second stage that raises the furnace temperature to the desired pyrolysis temperature (e.g., 500, 700 or 900 °C). After pyrolysis reached the final heat treatment temperature, the furnace temperature was lowered, and the furnace cooled to ~150 °C before the crucibles were removed (Bollman, 2012).

2.2. Photochemical degradation of water-soluble biochar species

Photochemical degradation experiments involved subjecting biochar-water mixtures to artificial sunlight for 48 h (equivalent to 8 days of natural sunlight) in a solar simulator, with dark controls wrapped in foil for comparison (Chen et al., 2022). Fig. S1 shows a picture of the biochar and water microcosms. Details are available in the supporting information.

2.3. Surface morphology

The sample morphology of low (300 °C) and high (900 °C) temperature biochar, after water-washing with and without photo-irradiation, were imaged by scanning electron microscopy (SEM) on a Thermo-Fisher Dualbeam Helios G4 SEM microscope equipped with an Oxford Aztec SDD energy dispersive X-ray spectroscopy (EDS) detector. The dried samples were spread on a conductive carbon adhesive tape surface attached to an SEM sub without coating. The secondary electron images were taken using the following imaging conditions: 2 kV voltage, around 4.00 mm working distance, and a beam current of 0.10 nA. The EDS spectrum was collected from the sample at 20 kV with a beam current of 0.4 nA to ensure voltages above the element excitation energy level for EDS peak detection.

2.4. Dissolved organic carbon (DOC) measurement

Each sample was filtered through a 0.45 µm nylon filter to remove undissolved biochar. DOC measurements for water-soluble species from each biochar were measured at the University of Georgia stable Isotope Ecology Laboratory using a Shimadzu TOC-5000A Total Organic Carbon Analyzer and Shimadzu TOC-Vcsh (Shimadzu Corp., Japan). The mean of the two injections was recorded for every sample, and the coefficient of variance (CV) was within 2 % for replicate injections.

2.5. Acute toxicity analysis of water-soluble species

Microtox® toxicity analysis was used to track the toxicity of water-soluble biochar species generated before and after 48 h irradiation (Pelletier et al., 2004). Water samples from both test and control microcosms were carbon normalized to 33.19 ppm (the lowest DOC concentration of the sample set) prior to Microtox® testing. The decrease in the bioluminescence of *Aliivibrio fischeri* bacteria after a 15-min incubation period establishes the toxicity of each water fraction through the measurement of light emitted by the bacteria. The Microtox® 81.9% screening test protocol was used on the Microtox® model 500 analyzer (Modern Water, New Castle, DE. USA) as described previously (Chen et al., 2022). To compare the toxicity of biochar produced at different temperatures (300 °C, 500 °C, 700 °C, and 900 °C) under dark and irradiated conditions, an ANOVA (Analysis of Variance) test was performed, and p-values were calculated to determine if there were statistically significant differences between the dark and irradiated samples at each temperature.

2.6. Solid phase extraction of water-soluble organics (WSO)

After 48 h (i.e., stirring in the dark or being photo-irradiated), water was transferred via glass pipettes and filtered (0.45 µm nylon filter) to remove undissolved biochar. Approximately ~20 mL of filtered water was acidified to pH 2 with trace-metal free HCl, followed by solid-phase extraction (SPE) with a C_{18} column (Agilent Technologies) (Dittmar et al., 2008). WSO were eluted with methanol and stored in pre-combusted borosilicate vials (DWK Life Sciences Wheaton™ Clear Glass Sample Vials) at 4 °C in the dark prior to FT-ICR mass spectral analysis.

2.7. Negative-ion electrospray ionization 21 T FT-ICR mass spectrometry and data analysis

All samples were analyzed by negative-ion electrospray ionization on a custom-built hybrid linear ion trap/21 T FT-ICR mass spectrometer at the National High Magnetic Field Laboratory (Hendrickson et al., 2015; Bahureksa et al., 2022). Complete experimental details can be found in the Supporting Information. All 21-T FT-ICR MS files and assigned elemental compositions are publicly available via the Open Science Framework (https://osf.io/v3wb7/) at DOI 10.17605/OSF.IO/V3WB7.

2.8. Environmentally relevant compounds screening

A list of the top 100 elemental compositions unique to the 300 °C Biochar sample that showed the largest change in toxicity after irradiation compared to the dark control was identified. A batch search was performed using the USEPA CompTox Chemicals Dashboard (https://comptox.epa.gov/dashboard) to identify potential environmentally and public health-relevant compounds (Lowe and Williams, 2021).

3. Results and discussion

3.1. Morphology changes in biochar after irradiation

A comparison of surface morphology of 300 °C and 900 °C biochar after water-washing with and without solar irradiation by scanning electron microscopy (SEM) is shown in Fig. S2. Previous studies report loss of salt and organic biochar coating after water washing for 24 h (Spokas et al., 2014), which would enable observation of surface characteristics throughout biochar processing. Fig. S2 highlights surface morphology differences after 48 h of water-washing, with and without photo-irradiation. Importantly, the porous structure of the wheat straw is different between the 300 °C sample and the 900 °C sample: the 300 °C residue has smaller, more compact pores, whereas the 900 °C residue contains large, well-formed pores. Due to charging, it was difficult to image the 300 °C sample, as the image distorted at higher magnification (Figs. S2a and S2b), indicating insulating properties. Conversely, the lack of bright spots on the 900 °C sample indicated that it is conductive (Figs. S2c and S2d). Constant surface morphology was observed between non-irradiated and irradiated 900 °C biochar samples, indicating an insignificant impact of solar irradiation on biochar surface morphology.

3.2. Quantitative trends in production of water-soluble carbon: impact of temperature and solar irradiation

The amount of water-soluble biochar species generated at each temperature and the impact of solar irradiation was evaluated for all fractions, reported as dissolved organic carbon concentration (DOC). Fig. 1 shows the fraction of dissolved organic carbon (DOC) from biochar manufactured at each temperature in dark and irradiated microcosms. A more than five-fold increase in DOC was observed at 300 °C with solar irradiation, from 33.2 mg C L^{-1} to 181.9 mg C L^{-1}. Nearly three times the amount of DOC was formed after solar irradiation at 500 °C, from 36.5 mg C L^{-1} to 98.8 mg C L^{-1}. Surprisingly, DOC values from 700 °C resulted in little change in DOC, from 46.5 mg C L^{-1} to 51.4 mg C L^{-1}, whereas 900 °C biochar resulted in a slightly lower amount of DOC after irradiation, from 71.0 mg C L^{-1} to 53.1 mg C L^{-1}. Notably, the DOC of the dark samples increased from 33.2 mg C L^{-1} at 300 °C to 53.1 mg C L^{-1} at 900 °C, indicating that higher pyrolysis temperatures resulted in a greater quantity of water-soluble organic compounds in a biochar. This trend suggests that thermal decomposition processes at higher temperatures produce more labile and soluble fractions, potentially enhancing the bioavailability of organic carbon in environmental applications. Trends in DOC highlight compositional differences in biochar as a function of pyrolysis temperature, which determines the degree of photoreactivity and subsequent DOC generation (Bostick et al., 2018; Wozniak et al., 2020).

3.3. Trends in toxicity of WSO-biochar species after photodegradation

Water-soluble fractions derived from all eight microcosms (four temperatures, dark and irradiated) were analyzed by Microtox® to evaluate general trends in toxicity impacted by photoirradiation (Chen et al., 2022). Microtox® analysis is a widely utilized *in vitro* testing method that uses bioluminescent bacteria (*Allivibrio fischeri*) to detect toxic substances in different environmental matrices (e.g., water, air, soils, and sediment) (Doherty, 2001). Bioluminescence inhibition, measured per carbon unit, corresponds to increased acute toxicity. Fig. 2 shows the acute toxicity of water-soluble species per unit of carbon. Under solar irradiation, water-soluble 300 °C biochar species are more than two-fold toxic than their dark counterparts, with an increase in acute toxicity from 19% to 50%, and a slight increase in toxicity observed at 700 °C, from 9% to 11% inhibition. At 900 °C, toxicity tripled for irradiated WSO species compared to dark analogs from 4% to 12% inhibition. Importantly, toxicity *decreased* after irradiation for 500 °C-derived WSO species from 13% to 10%. The disparity in toxicity trends for wheat straw biochar formed at different temperatures after solar irradiation suggests that wheat straw biochar produced at 500 °C will minimize deleterious effects that occur as biochar is photodegraded. ANOVA analysis indicates that at temperatures 300 °C, 500 °C, and 900 °C, there are statistically significant differences in toxicity between the dark and irradiated samples (p-value <0.05). However, at 700 °C, no significant difference was observed (p-value >0.05). These findings highlight the significant impact of pyrolysis temperature and photodegradation on the toxicity of biochar. Notably, the largest changes in toxicity were observed at 300 °C and 900 °C.

3.4. Compositional evaluation of photoirradiated water-soluble biochar fractions: negative-ion ESI 21 T FT-ICR MS

3.4.1. Mass spectral complexity

Fig. S3 shows broadband (full mass range) negative ion ESI 21 T FT-ICR mass spectra for water-soluble fractions derived from 300 °C biochar after 48 h with and without irradiation. The achieved mass resolving power (m/Δm$_{50\%}$, in which Δm$_{50\%}$ is mass spectral peak full width at half-maximum peak height) (Marshall et al., 1998) for both spectra is 2,750,000 at m/z 200, which enables the assignment of ~11,000 species (RMS error = 5 ppb; 48 h, dark) and ~35,000 species (RMS error = 38
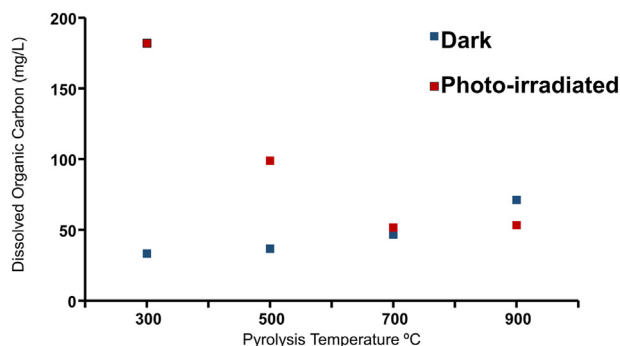

Fig. 1. Dissolved organic carbon (DOC) concentration of 20 mL water samples after 48 h water-washing versus pyrolysis temperature with (red) and without (blue) solar irradiation, presented as the mean of two measurements (RSD <2%).
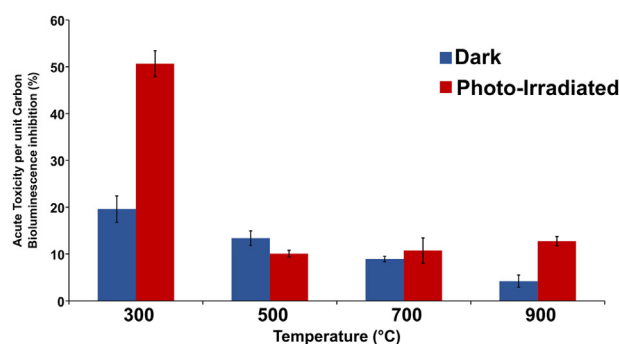

Fig. 2. Acute toxicity per unit carbon bioluminescence inhibition (%) for water-soluble fractions derived from wheat straw biochar pyrolyzed at 300, 500, 700, and 900 °C, based on 15 min bioluminescence inhibition measured in triplicates.

ppb; 48 h, irradiated). The mass-scale expanded zoom inset (Fig. S3A) (m/z 670) further highlights the spectral density, with ~42 peaks within a 300 mDa window. Further mass-scale expansion is shown in Fig. S3B, with ~9 peaks annotated with m/z, elemental composition, and mass error. Here, the achieved resolving power enabled the baseline resolution of species with the same nominal mass that differ in exact mass by 2.1 mDa ($C_{30}H_{26}N_1O_{17}$ versus $C_{16}H_{35}O_{25}S_1^{13}C_1$), approximately the mass of four electrons (0.54 mDa) that would be unresolved by any other mass analyzer (Roth et al., 2022). The polydispersity, polyfunctionality, and compositional complexity of biochar require ultrahigh resolving power (McKenna et al., 2021; Bahureksa et al., 2022).

3.4.2. Impact of photodegradation and pyrolysis temperature on biochar WSO composition

Heteroatom class distributions group all species based on the type and number of heteroatoms (e.g., oxygen, nitrogen, sulfur) identified in a mass spectrum and provide rapid visualization of compositional trends for the sample analyzed similarly (Rodgers and Marshall, 2007). Fig. 3 shows the heteroatom class distribution for oxygen classes derived from negative-ion ESI 21 T FT-ICR MS for WSO species generated after 48 h in the dark (Fig. 3a) and with solar irradiation (Fig. 3b). The most abundant species in the water-soluble fractions derived from the 300 °C biochar (48 h, irradiated) contain up to 30 oxygen atoms. In contrast, the species in the dark samples pyrolyzed at the same temperature contain an average of approximately 10 fewer oxygen atoms per molecule (O_{17}–O_{20}). On average, the oxygen classes have lower oxygen content per molecule without solar irradiation. The most abundant classes were O_{12}–O_{16} in irradiated samples (300°) which differed from the dominant O_6–O_9 species in the dark samples. Additionally, the abundance of NOx compounds was evaluated and compared to Ox compounds. The data indicates that NOx compounds are less abundant than Ox compounds across all samples. Specifically, the relative abundance of NOx compounds is approximately 20% of the total Ox compounds. This trend remains consistent regardless of the pyrolysis temperature or irradiation conditions. This agrees with a previous study that reported the production of toxic oxy-PAHs and similar photoproducts from photodegraded biochar (Lampi et al., 2009). Increases in oxygen-containing functional groups are also noted in laboratory biotic-aged biochar (Quan et al., 2020). Both 500 °C biochar-derived WSO fractions are dominated by O_7–O_{11} classes, with a shift to higher oxygen number (O_{16}–O_{20}) with solar irradiation. A similar trend occurred in the 700 °C biochar, but photoproducts span higher oxygen classes (O_{15}–O_{19}) and are more abundant than their dark counterparts. At 900 °C, dark and photo-generated water-soluble biochar species correspond to the same O_x class distribution, with dark species (O_{11}–O_{13}) slightly more oxidized than photoproducts. In negative-ion ESI, the O_1 class corresponds to phenol and/or alcohols, which are reactive intermediates in the photo-degradation of organic species, and although the largest change in toxicity occurred at 300 °C, future studies will evaluate various feedstocks at lower pyrolysis temperatures.

3.4.3. Van Krevelen diagrams of H/C versus O/C

Because FT-ICR MS assigns tens of thousands of species in a single mass spectrum, graphical representation of elemental compositions allows for rapid visualization of qualitative changes between samples and is widely applied to natural organic matter systems (e.g., biochar) to highlight global shifts in atomic H/C ratio (y-axis) and O/C ratio (x-axis) (van Krevelen, 1950). Van Krevelen diagrams generated from FT-ICR MS data sets provide visualization of the approximate oxidation state (Boye et al., 2017), compositional information to biomolecular precursors, and hydrogen deficiency (McLafferty and Turecek, 1993), or aromaticity index (Koch et al., 2007; AI) to approximate biolability (Kim et al., 2003; D'Andrilli et al., 2013; Minor et al., 2014; Rivas-Ubach et al., 2018). Natural organic matter systems include biochar and oxidized black carbon (Hertkorn et al., 2006; Stubbins et al., 2010) that typically exhibit hydrogen saturation and oxygenation as 0 < H/C < 2.5 and 0 < O/C < 1.0. In a van Krevelen diagram, species cluster into regions corresponding to compound classes, aromaticity, and possible chemical reaction pathways for particular ranges of H/C and O/C ratios (Kim et al., 2003). Proposed stoichiometric and elemental constraints for compound classes in natural organic matter are categorized by multidimensional stoichiometric compounds classification (MSCC) (Rivas-Ubach et al., 2018) as follows: lipids (O/C ≤ 0.6; H/C ≥ 1.32); peptides (0.12 < O/C ≤ 0.6; 0.9 < H/C < 2.5) and (0.6 < O/C ≤ 1; 1.2 < H/C < 2.5); amino sugars (O/C ≥ 0.61; H/C ≥ 1.45); carbohydrates (O/C ≥ 0.8; 0.167 ≤ H/C < 2.7); nucleotides 0.5 ≤ O/C < 1.7; 1 < H/C < 1.8) phytochemical compounds and lignin (O/C ≤ 1.15 and H/C < 1.32); and condensed hydrocarbons (0.01 < O/C < 0.25; 0.2 < H/C < 1.4) (Kim et al., 2003; D'Andrilli et al., 2013; Minor et al., 2014).

Fig. 4 shows van Krevelen diagrams of H/C versus O/C for neutral oxygen-containing (O_x) species unique to WSO generated after 48 h. Each data point corresponds to a unique monoisotopic elemental composition, with aromaticity index color-coded: non-aromatic (black, A.I. ≤ 0.5), aromatic (blue, 0.67 > A.I. > 0.5), and condensed aromatic (red, A.I. ≥
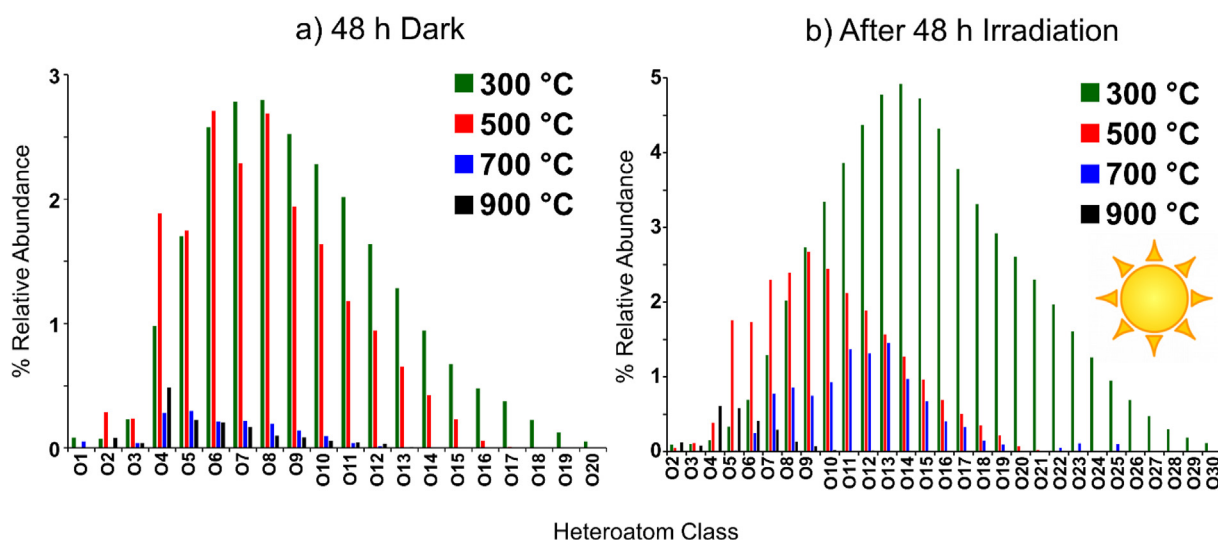

Fig. 3. Heteroatom class distribution for O_x species derived from negative-ion electrospray ionization 21 T FT-ICR MS for water-soluble fractions derived from wheat straw biochar produced at 300, 500, 700, and 900 °C in 48 h dark (a) and 48 h irradiated (b).
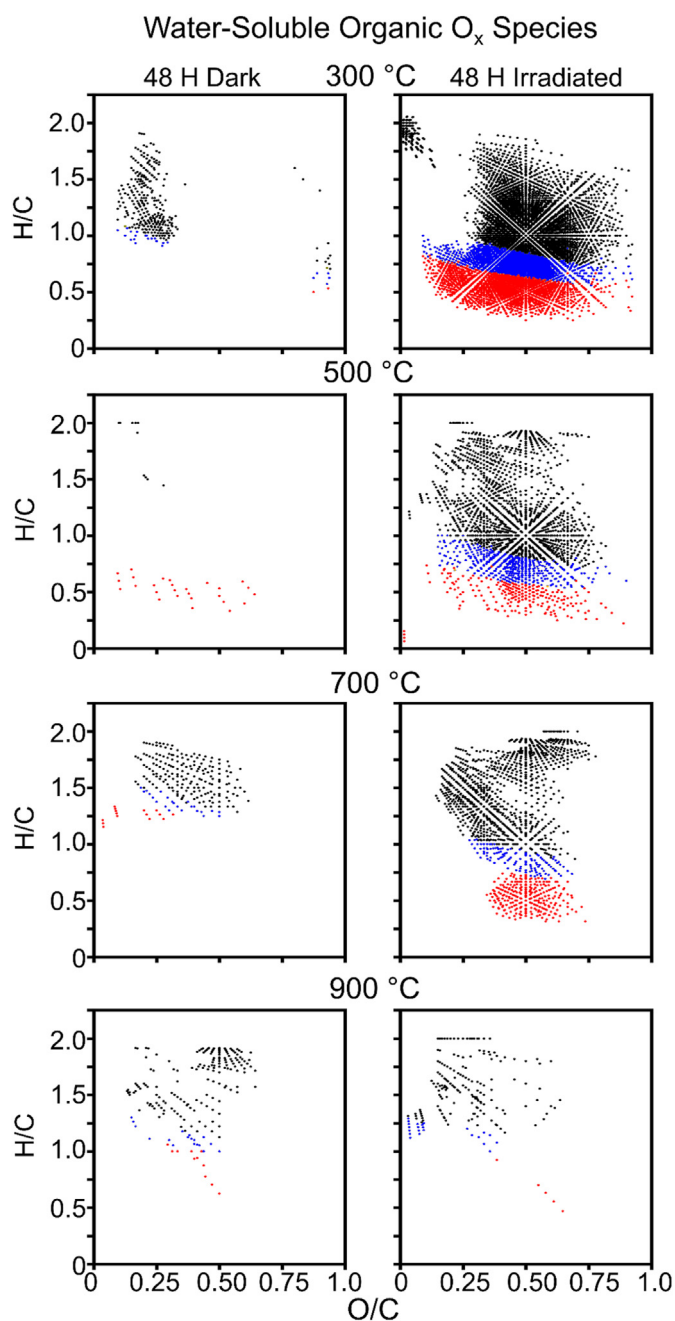
Water-Soluble Organic O_x Species

Fig. 4. van Krevelen diagram of atomic H/C versus O/C for neutral oxygen (O_x) species unique to WSO generated in the dark (left) and after irradiation (right). Each data point corresponds to a unique elemental composition and is color-coded by aromaticity index (A.I.): non-aromatic (black, A.I. ≤ 0.5), aromatic (Blue, $0.67 > $ A.I. > 0.5), and condensed aromatic (red, A.I. ≥ 0.67).

0.67). At 300 °C, wheat straw biochar generated water-soluble species in the dark that correspond to lower aromaticity indices (non-aromatic, black), with O/C $= 0.10$–0.30 and H/C $= 1.0$–1.8. Unique WSO species detected after irradiation corresponds to calculated aromaticity indices across a range of saturation (non-aromatic (black), aromatic (blue), and condensed aromatic (red)), with H/C ratios $= 0.25$–1.75 and O/C ratios $= 0.1$–0.8. Most condensed (red) and aromatic (blue) species generated through irradiation were observed at 300, 500, and 700 °C, but very few of these species were observed in WSO fractions derived from 900 °C biochar. The widest range of H/C and O/C ratios was observed after irradiation for 300 and 500 °C biochar, with species from H/C $= 0.1$–2.0 and O/C $= 0.1$–0.8, and comprises a broad range of chemical

functionality (Waggoner et al., 2015), whereas 700 °C biochar WSO has a more defined in O/C ratio of 0.2–0.75.

3.4.4. Carbon number dependence of 300 °C biochar photoproducts water solubility: H/C and O/C ratio versus carbon number

Water-soluble species derived from the irradiated 300 °C biochar were almost three times more toxic than non-irradiated analogs. Therefore, we focused on identifying the molecular signature of newly formed species in the 300 °C biochar. It is important to note that 300 °C is relatively low for typical pyrolysis processes, generally occurring at temperatures above 400 °C. The selection of 300 °C in this study was intended to investigate the lower end of the thermal degradation spectrum, providing insights into the changes in biochar properties and composition at sub-pyrolytic temperatures. This helps to better understand the transition from biomass to biochar and the resulting impact on water-soluble species.

Fig. 5a shows the H/C ratio versus carbon number for both water-soluble fractions of 300 °C biochar, with relative abundance color-coded for the most abundant species in each mass spectrum. Relative abundance-weighted average carbon number, H/C ratio, and DBE are shown on each image. Water-soluble O_x species after irradiation extend to C_{70}, whereas dark species are smaller and contain $< C_{50}$ and higher H/C ratio (Chen et al., 2014). A shift from H/C of 1.1 to 0.95 observed with irradiation indicates the presence of more conjugated, aromatic, and hydrogen-deficient species (e.g., OxyPAHs and PAXHs), which could contribute to increased acute toxicity (Lampi et al., 2009). Smith et al. (2013) employed (−) ESI FT-ICR MS to analyze the biochar water extracts and suggest that degraded lignin-like species, rich in oxygen-containing functionalities also identified in our irradiated 300 °C biochar samples, are most likely the inhibitor species for aquatic photosynthetic microorganism growth. Another possible explanation is that aggregated species contribute to the DOC and further degrade into smaller species that are identified by FT-ICR MS. For the current study, we are focusing on small molecules (<1500 Da) that exist primarily as monomers.

O/C Ratio: Dark vs Irradiated. Fig. 5b plots the O/C ratio versus carbon number for water-soluble biochar species to investigate the relationship between carbon number and degree of oxidation (O/C). Dark WSO species contain C_{10}–C_{52} (average C_{26}), whereas photoproducts are larger (C_{10}–C_{70}), with a higher average O/C ratio (O/C 0.46), compared to dark (O/C 0.39. Dark-derived WSO had a marginally higher O/C (($0.1 < $ O/C < 1.3) compared to photoproducts ($0.1 < $ O/C < 1.0).

DBE. DBE, or the number of double bonds and rings to carbon, is calculated from the elemental composition and is a measure of aromaticity for a molecule (McLafferty and Turecek, 1993). Irradiated WSO biochar species are more aromatic (higher DBE at the same carbon number) (DBE 20) compared to dark species (DBE 15), with higher carbon number, lower H/C ratio, and higher O/C, which could indicate polymerization of dissolved organic species and will be further investigated in subsequent studies (Chen et al., 2014). Additional compositional images are shown in the Supporting Information. DBE versus carbon number for O_x dark species and O_x photoproducts (Fig. S4) and N_1O_x (Fig. S5) from the 300 °C biochar.

3.4.5. Potential chemical identification of 300 °C biochar photoproducts using EPA CompTox Chemicals Dashboard

The top 100 unique formulae unique to the 300 °C biochar sample were subjected to a batch search using a research version of the CompTox Chemicals Dashboard (from hereon, the Dashboard) with data contained in the DSSTox database (https://doi.org/10.1016/j.comtox.2019.1000 96) for the most recent data available up to March 4th, 2023. The batch search, based on MS-Ready formulae (https://jcheminf.biomedc entral.com/articles/10.1186/s13321-018-0299-2) yielded a list of 20 potential chemical structures, which is detailed in Table S1. This list highlights certain recurring features among the chemicals, notably the presence of glucopyranoside rings and esterified aromatic rings,
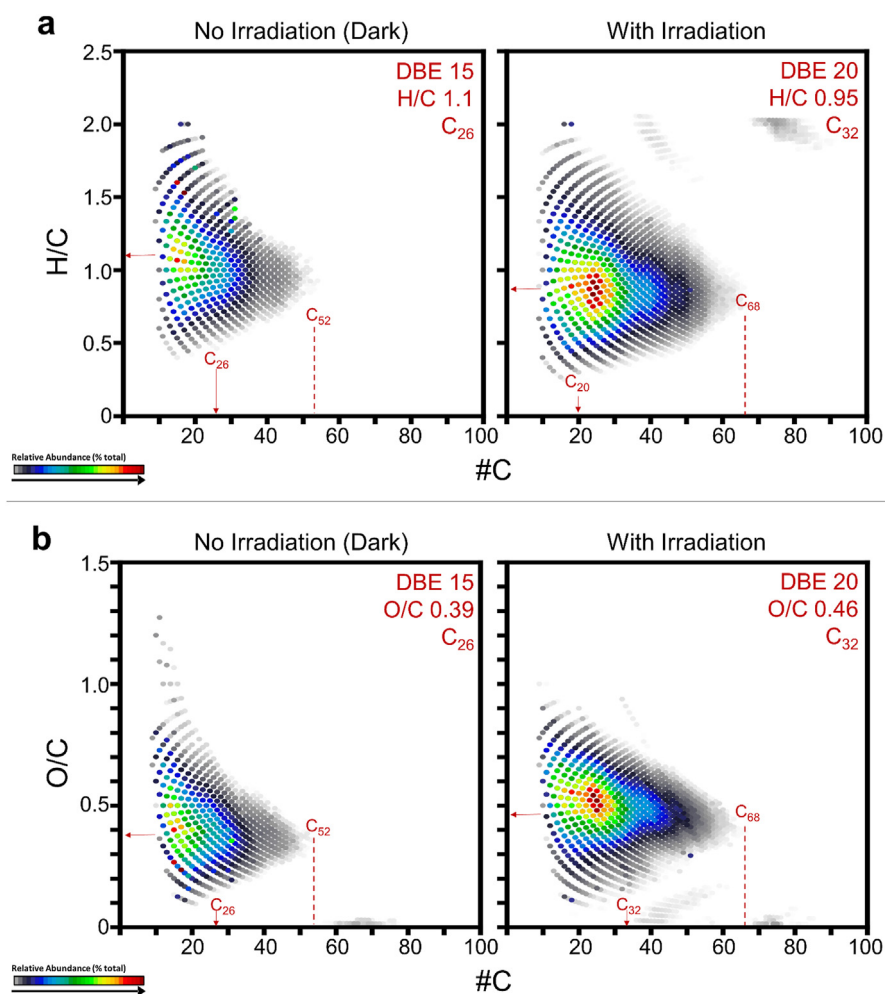
Fig. 5. H/C vs. carbon number plots (a) and O/C ratio vs. carbon number (b) derived from (−) ESI FT-ICR MS on the water-soluble species of the dark and irradiated wheat straw biochar generated at 300 °C.

suggesting commonalities within this chemical set. The set of chemicals was then processed through the Hazard Comparison Module of the public cheminformatics modules tool (https://www.epa.gov/comptox-tools/cheminformatics), suggesting that many of the chemicals would have very high acute aquatic ecotoxicity (Fig. S6), consistent with the observed heightened toxicity in the 300 °C biochar photoproducts. Among the 20 potential chemical structures identified, a notable fraction contains glycosylated compounds. These glycosylated species suggest a more complex chemical landscape than originally anticipated. While we previously emphasized the role of degraded lignin-like species in contributing to toxicity, it is important to acknowledge that the glycosylated compounds may also play a role. Their potential degradation products or interactions with other compounds in the mixture could influence the observed toxicity. Therefore, both lignin-like and glycosylated species should be considered when evaluating the toxic potential of the photoproducts formed at 300 °C. Nevertheless, it is important to acknowledge the inherent limitations of using both Dashboard tools and chemical databases, which are not comprehensive, for the interpretation of FT-ICR MS data. FT-ICR MS data primarily provides molecular formula assignments, offering valuable insights into the elemental composition of compounds present in a sample. However, when it comes to interpreting compound structures and assessing environmental toxicity, caution is warranted.

Additional resources and experimental validation are needed to ensure accurate characterization and evaluation of potential environmental risks of the compounds identified.

4. Conclusions

Although minimal alteration of biochar surface morphology was observed through photo-irradiation, the greatest amount of water-soluble species leached from photo-irradiated biochar at 300 °C. FT-ICR MS analysis revealed the molecular composition of the water-soluble species leached from biochar and showed that the photoproducts span a wider compositional space. A significant increase in acute toxicity was observed in 300 °C and 900 °C biochar samples after 48 h of photoirradiation, which correlated with the increased relative abundance of higher-order oxygenated species (O_{28}–O_{30}). While some of these species are likely toxic oxy-PAH photoproducts, as suggested by the ComTox Chemicals Dashboard, only a fraction of the identified structures include the characteristic quinone rings typical of oxy-PAHs. The majority of the structures represent other oxygenated compounds, which may also contribute to the observed toxicity. The study uses advanced analytical techniques to reveal the impact of photooxidation on the toxicity and molecular composition of water-soluble species across

biochar pyrolysis temperatures. More importantly, this study illustrates that biochar-derived dissolved organic carbon has the potential to form a wide range of toxic aquatic species due to photooxidation, not limited to oxy-PAHs. This field warrants further exploration to fully understand the environmental implications of biochar applications.

Data availability

All FT-ICR MS spectra files (.pfd) and elemental composition assignments (.xls) are publicly-available via the Open Science Framework (https://osf.io/v3wb7/) at DOI 10.17605/OSF.IO/V3WB7 in accordance with the NHFML and NSF FAIR data management plan (https://nationalmaglab.org/images/user_resources/searchable_docs/request_magnet_time/data_management_plan_policy.pdf). Any additional reasonable requests for information will be provided by the corresponding authors.

CRediT authorship contribution statement

Amy M. McKenna: Writing – review & editing, Writing – original draft, Visualization, Methodology, Investigation, Funding acquisition, Formal analysis, Data curation, Conceptualization. **Martha L. Chacón-Patiño:** Writing – review & editing, Visualization, Methodology. **Holly K. Roth:** Writing – review & editing, Methodology. **William Bahureksa:** Writing – review & editing, Methodology. **Robert B. Young:** Writing – review & editing, Methodology. **James A. Ippolito:** Writing – review & editing, Methodology, Funding acquisition. **Yan Xin:** Writing – review & editing, Methodology. **Thomas Borch:** Writing – review & editing, Resources, Methodology, Funding acquisition, Conceptualization. **Antony J. Williams:** Writing – review & editing, Methodology, Formal analysis. **Huan Chen:** Writing – review & editing, Visualization, Methodology, Investigation, Formal analysis, Data curation, Conceptualization.

Declaration of competing interest

The views expressed in this manuscript are solely those of the authors and do not represent the policies of the US EPA. Mention of trade names of commercial products should not be interpreted as an endorsement by the US EPA. This work has been internally reviewed at the US EPA and has been approved for publication. The authors declare that they have no known competing financial interests or personal relationships that could have appeared to influence the work reported in this paper.

Appendix A. Supplementary data

Supplementary data to this article can be found online at https://doi.org/10.1016/j.seh.2024.100114.

References

Ahmed, A., Kurian, J., Satyanarayana, S., Raghavan, V., 2021. Impact of wood-derived biochar on the hydraulic characteristics of compacted soils: its influence on simulated farmland carbon sequestration. Int. Agrophys. 35 (2), 167–177.

Awan, S., Ippolito, J.A., Ullman, J.L., Ansari, K., Cui, L., Siyal, A.A., 2021. Biochars reduce irrigation water sodium adsorption ratio. Biochar 3, 77–87. https://doi.org/10.1007/s42773-020-00073-z.

Bahureksa, W., Borch, T., Young, R.B., Weisbrod, C.R., Blakney, G.T., McKenna, A.M., 2022. Improved dynamic range, resolving power, and sensitivity achievable with FT-ICR mass spectrometry at 21 T revelas the hidden complexity of natural organic matter. Anal. Chem. 94 (32), 11382–11389. https://doi.org/10.1021/acs.analchem.2c02377.

Bahureska, W., Tfaily, M.M., Boiteau, R.M., Young, R.B., Logan, M.N., McKenna, A.M., Borch, T., 2021. Soil organic matter characterization by Fourier transform ion cyclotron resonance mass spectrometry (FT-ICR MS): a critical review of sample preparation, analysis, and data interpretation. Environ. Sci. Technol. 55 (14), 9637–9656. https://doi.org/10.1021/acs.est.1c01135.

Bare, W.F.R., Struhs, E., Mirkouei, A., Overturf, K., Chacón-Patiño, M.L., McKenna, A.M., et al., 2023. Controlling eutrophication of aquaculture production water using biochar: correlation of molecular composition with adsorption characteristics as revealed by FT-ICR mass spectrometry. Processes 11 (10), 2883.

Bednik, M., Medyńska-Juraszek, A., Ćwielag-Piasecka, I., 2022. Effect of six different feedstocks on biochar's properties and expected stability. Agronomy 12, 1525. https://doi.org/10.3390/agronomy12071525.

Bollman, M.A., 2012. Standard Operating Procedure for Biochar Preparation. U.S.E.P. Agency.

Bostick, K.W., Zimmerman, A.R., Goranov, A.I., Mitra, S., Hatcher, P.G., Wozniak, A.S., 2021. Photolability of pyrogenic dissolved organic matter from a thermal series of laboratory-prepared chars. Sci. Total Environ. 724, 1–9. https://doi.org/10.1016/j.scitotenv.2020.138198.

Bostick, K.W., Zimmerman, A.R., Wozniak, A.S., Mitra, S., Hatcher, P.G., 2018. Production and composition of pyrogenic dissolved organic matter from a logical series of laboratory-generated chars. Front. Earth Sci. https://doi.org/10.3389/feart.2018.00043.

Boye, K., Noël, V., Tfaily, M.M., Bone, S.E., Williams, K.H., Bargar, J.R.R., Fendorf, S., 2017. Thermodynamically controlled preservation of organic carbon in floodplains. Nat. Geosci. 10 (6), 415–419.

Chen, H., Abdulla, H.A.N., Sanders, R.L., Myneni, S.C.B., Mopper, K., Hatcher, P.G., 2014. Production of black carbon-like and aliphatic molecules from terrestrial dissolved organic matter in the presence of sunlight and iron. Environ. Sci. Technol. Lett. 1 (10), 399–404.

Chen, H., McKenna, A.M., Niles, S.F., Frye, J.W., Glattke, T.J., Rodgers, R.P., 2022. Time-dependent molecular progression and acute toxicity of oil-soluble, interfacially-active, and water-soluble species reveals their rapid formation in the photodegradation of Macond Well Oil. Sci. Total Environ. 813, 151884. https://doi.org/10.1016/j.scitotenv.2021.151884.

Coppola, A.I., Wiedemeier, D.B., Galy, V., Haghipour, N., Hanke, U.M., Nascimento, G.S., et al., 2018. Global-scale evidence for the refractory nature of riverine black carbon. Nat. Geosci. 11 (8), 584–588.

D'Andrilli, J., Foreman, C.M., Marshall, A.G., McKnight, D.M., 2013. Characterization of IHSS pony lake fulvic acid dissolved organic matter by electrospray ionization fourier transform ion cyclotron resonance mass spectrometry and fluorescence spectroscopy. Org. Geochem. 65, 19–28.

Dittmar, T., Koch, B., Hertkorn, N., Kattner, G., 2008. A simple and efficient method for the solid-phase extraction of dissolved organic matter (SPE-DOM) from seawater. Limnol Oceanogr. Methods 6, 230–235. https://doi.org/10.4319/lom.2008.6.230.

Doherty, F.G., 2001. A review of the Microtox® toxicity test system for assessing the toxicity of sediments and soils. Water Qual. Res. J. Can. 36 (3), 475–518.

Dutta, T., Kwon, E., Bhattacharya, S.S., Jeon, B.H., Deep, A., Uchimiya, M., Kim, K.H., 2017. Polycyclic aromatic hydrocarbons and volatile organic compounds in biochar and biochar-amended soil: a review. Gcb Bioenergy 9 (6), 990–1004.

Godlewska, P., Ok, Y.s., Oleszczuk, P., 2021. The dark side of black gold: ecotoxicological aspects of biochar and biochar-amendedsoils. J. Hazard Mater. 403, 123833. https://doi.org/10.1016/j.jhazmat.2020.123833.

Han, H., Buss, W., Zheng, Y., Song, P., Khalid, R.M., Liu, P., et al., 2022. Contaminants in biochar and suggested mitigation measures — a review. Chem. Eng. J. 429, 132287. https://doi.org/10.1016/j.cej.2021.132287.

Hendrickson, C.L., Quinn, J.P., Kaiser, N.K., Smith, D.F., Blakney, G.T., Chen, T., et al., 2015. 21 Tesla Fourier transform ion cyclotron resonance mass spectrometer: a national resource for ultrahigh resolution mass analysis. J. Am. Soc. Mass Spectrom. 26 (9), 1626–1632.

Hertkorn, N., Benner, R., Frommberger, M., Schmitt-Kopplin, P., Witt, M., Kaiser, K., et al., 2006. Characterization of a major refractory component of marine dissolved organic matter. Geochem. Cosmochim. Acta 70 (12), 2990–3010.

Hockaday, W.C., Purcell, J.M., Marshall, A.G., Baldock, J.A., Hatcher, P.G., 2009. Electrospray and photoionization mass spectrometry for the characterization of organic matter in natural waters: a qualitative assessment. Limnol Oceanogr. Methods 7 (1), 81–95.

Ippolito, J.A., Cui, L., Kammann, C., Wrage-Mönnig, N., Estavillo, J.M., Fuertes-Mendizabal, T., et al., 2020. Feedstock choice, pyrolysis temperature and type influence biochar characteristics: a comprehensive meta-data analysis review. Biochar 2, 421–438.

Kim, S., Kramer, R.W., Hatcher, P.G., 2003. Graphical method for analysis of ultrahigh-resolution broadband mass spectra of natural organic matter, the van Krevelen diagram. Anal. Chem. 75 (20), 5336–5344.

Koch, B.P., Dittmar, T., Witt, M., Kattner, G., 2007. Fundamentals of molecular formula assignment to ultrahigh resolution mass data of natural organic matter. Anal. Chem. 79 (4), 1758–1763. https://doi.org/10.1021/ac061949s.

Lampi, M.A., Gursk, J., McDonald, K.I.C., Xie, F., Huang, X.-D., Dixon, D.G., Greenberg, B.M., 2009. Photoinduced toxicity of polycyclic aromatic hydrocarbons to Daphnia magna: ultraviolet-mediated effects and the toxicity of polycyclic aromatic hydrocarbon photoproducts. Toxicol. Environ. Chem. 25 (4), 1079–1087. https://doi.org/10.1897/05-276R.1.

Liu, L., Fan, S., 2022. Effects of physical and chemical aging on polycyclic aromatic hydrocarbon (PAH) content and potential toxicity in rice straw biochars. Env. Sci. Pollut. Res. https://doi.org/10.1007/s11356-022-19869-6.

Lowe, C.N., Williams, A.J., 2021. Enabling high-throughput searches for multiple chemical data using the US-EPA CompTox chemicals dashboard. J. Chem. Inf. Model. 61 (2), 565–570.

Mao, J.D., Johnson, R.L., Lehmann, J., Olk, D.C., Neves, E.G., Thompson, M.L., Schmidt-Rohr, K., 2012. Abundant and stable char residues in soils: implications for soil fertility and carbon sequestration. Environ. Sci. Technol. 46 (17), 9571–9576. https://doi.org/10.1021/es301107c.

Marshall, A.G., Hendrickson, C.L., Jackson, G.S., 1998. Fourier transform ion cyclotron mass spectrometry: a primer. Mass Spectrom. Rev. 17 (1), 1–35.

McKenna, A.M., Chacón-Patiño, M.L., Chen, H., Blakney, G.T., Mentink-Vigier, F., Young, R.B., et al., 2021. Expanding the analytical window for biochar speciation: molecular comparison of solvent extraction and water-soluble fractions of biochar by FT-ICR mass spectrometry. Anal. Chem. https://doi.org/10.1021/acs.analchem.1c03058. Ahead of Print.

McLafferty, F.W., Turecek, F., 1993. Interpretation of Mass Spectra, fourth ed. University Science Books, Mill Valley, CA.

Minor, E.C., Swenson, M.M., Mattson, B.M., Oyler, A.R., 2014. Structural characterization of dissolved organic matter: a review od current techniques for isolation and analysis. Environ. Sci.: Process. Impacts 16, 2064–2079.

Pelletier, E., Delille, D., Delille, B., 2004. Crude oil bioremediation in the sub-Antarctic intertidal sediments: chemistry and toxicity of oiled residues. Mar. Environ. Res. 57 (4), 311–327.

Rivas-Ubach, A., Liu, Y., Bianchi, T.S., Tolić, N., Jansson, C., Paša-Tolić, L., 2018. Moving beyond the van Krevelen diagram: a new stoichiometric approach for compound classification in organisms. Anal. Chem. 90, 6152–6160.

Rodgers, R.P., Marshall, A.G., 2007. Petroleomics: advanced characterization of petroleum-derived materials by Fourier transform ion cyclotron resonance mass spectrometry (FT-ICR MS). In: Asphaltenes, Heavy Oils, and Petroleomics. Springer, pp. 63–93.

Rombolà, A.G., Fabbri, D., Meredith, W., Snape, C.E., Dieguez-Alonso, A., 2016. Molecular characterization of the thermally labile fraction of biochar by hydropyrolysis and pyrolysis-GC/MS. J. Anal. Appl. Pyrolysis 121, 230–239. https://doi.org/10.1016/j.jaap.2016.08.003.

Roth, H.K., Borch, T., Young, R.B., Bahureksa, W., Blakney, G.T., Nelson, A.R., et al., 2022. Enhanced speciation of pyrogenic organic matter from wildfires enabled by 21 T FT-ICR mass spectrometry. Anal. Chem. 94 (6), 2973–2980.

Schmidt, H.P., Kammann, C., Hagemann, N., Leifeld, J., Bucheli, T.D., Monedero, M.A.S., Cayuela, M.L., 2021. Biochar in agriculture –A systematic review of 26 global meta-analyses. GCB Bioenergy 00, 1–23. https://doi.org/10.1111/gcbb.12889.

Smith, C.R., Sleighter, R.L., Hatcher, P.G., Lee, J.W., 2013. Molecular characterization of inhibiting biochar water-extractable substances using electrospray ionization fourier transform ion cyclotron resonance mass spectrometry. Environ. Sci. Technol. 47 (23), 13294–13302.

Spokas, K.A., Cantrell, K.B., Novak, J.M., Archer, D.A., Ippolito, J.A., Collins, H.P., et al., 2012. Biochar: a synthesis of its agronomic impact beyond carbon sequestration. J. Environ. Qual. 41, 973–989. https://doi.org/10.2134/jeq2011.0069.

Spokas, K.A., Novak, J.M., Masiello, C.A., Johnson, M.G., Colosky, E.C., Ippolito, J.A., Trigo, C., 2014. Physical disintegration of biochar: an overlooked process. Environ. Sci. Technol. Lett. 1, 326–332 dx.doi.org/10.1021/ez500199t.

Stubbins, A., Spencer, R.G.M., Chen, H., Hatcher, P.G., Mopper, K., Hernes, P.J., et al., 2010. Illuminated darkness: molecular signatures of Congo River dissolved organic matter and its photochemical alteration as revealed by ultrahigh precision mass spectrometry. Limnol. Oceanogr. 55 (4), 1467–1477.

van Krevelen, D., 1950. Graphical-statistical method for the study of structure and reaction processes of coal. Fuel 29, 269–284.

Waggoner, D.C., Chen, H., Willoughby, A.S., Hatcher, P.G., 2015. Formation of black carbon-like and alicyclic aliphatic compounds by hydroxyl radical initiated degradation of lignin. Org. Geochem. 82, 69–76. https://doi.org/10.1016/j.orggeochem.2015.02.007.

Wang, C., Wang, Y., Herath, H.M.S.K., 2017. Polycyclic aromatic hydrocarbons (PAHs) in biochar – their formation, occurrence and analysis: a review. Org. Geochem. 114, 1–11. https://doi.org/10.1016/j.orggeochem.2017.09.001.

Ward, C.P., Sleighter, R.L., Hatcher, P.G., Cory, R.M., 2014. Insights into the complete and partial photooxidation of black carbon in surface waters. Environ. Sci. J. Integr. Environ. Res.: Process. Impacts 16 (4), 721–731.

Wozniak, A.S., Goranov, A.I., Mitra, S., Bostick, K.W., Zimmerman, A.R., Schlesinger, D.R., et al., 2020. Molecular heterogeneity in pyrogenic dissolved organic matter from a thermal series of oak and grass chars. Org. Geochem. 148, 104065. https://doi.org/10.1016/j.orggeochem.2020.104065.

Xiang, L., Liu, S., Ye, S., Yang, H., Song, B., Qin, F., et al., 2021. Potential hazards of biochar: the negative environmental impacts of biochar applications. J. Hazard Mater. https://doi.org/10.1016/j.jhazmat.2021.126611. Ahead of print.

Zhang, K., Sun, P., Khan, A., Zhang, Y., 2021. Photochemistry of biochar during ageing process: reactive oxygen species generation and benzoic acid degradation. Sci. Total Environ. 765, 144630. https://doi.org/10.1016/j.scitotenv.2020.144630.